Chemical Physics xxx (xxxx) 111479

Contents lists available at ScienceDirect

Chemical Physics

journal homepage: www.elsevier.com/locate/chemphys

High-pressure crystal polymorphs and multiple pathways in 1-hexyl-3-methylimidazolium perfluorobutanesulfonate ionic liquid

Hiroshi Abe [a,*], Yoshihiro Koyama [b], Seiya Shimono [a], Hiroaki Kishimura [a], Kiyoto Matsuishi [b]

[a] Department of Materials Science and Engineering, National Defense Academy, Yokosuka 239-8686, Japan
[b] Graduate School of Pure and Applied Science, University of Tsukuba, Tsukuba 305-8573, Japan

ARTICLE INFO

Keywords:
Fluorinated ionic liquid
Crystal polymorph
Multiple pathways
Molecular conformations
Reentrant layering

ABSTRACT

1-Hexyl-3-methylimidazolium perfluorobutanesulfonate ([C_6mim][PFBS]), a fluorinated ionic liquid (fIL), exhibited complicated phase behaviors under high pressure (HP). The asymmetric [PFBS]$^-$ anion possesses conformational degrees of freedom. Using X-ray diffraction, HP crystal structures were determined upon compression and decompression. 00ℓ Bragg reflections at the small scattering angle representing the layered structures appeared reentrantly. The reentrant phase behavior is described by layering of [PFBS]$^-$ (*layering* I) below 3.7 GPa (P_1) and the hybrid layered structure of [PFBS]$^-$ (*layering* II) above 7.6 GPa. The *layering* II caused irreversible crystal polymorph in the pressure cycle. Below P_1, HP-phase transition changed to reversible crystal polymorph. The complicated HP-crystal polymorphs and multiple pathways were derived from the conformation-driven molecular packing states.

1. Introduction

Crystal polymorphs in a molecular system have been attracted for a long time on the fundamental science [1–4]. As geometrical degrees of freedom, the molecular conformations in crystal including a metastable phase provide a fingerprint to clarify the stabilization mechanism in the crystal states. Questions about crystal polymorphs of the molecular basis materials were open to the public [3]. From the viewpoint of structure and property, molecular conformations control the molecular-inherent functionalities. To search for possible crystal structures permitting various molecular conformations, crystal structure prediction (CSP) studies have been developed using computers [5,6]. The concept of crystal energy landscape [7,8] was introduced in CSP. Then, the CSP was applied to the pharmaceutical polymorph screening [9,10]. It is a serious problem that the physicochemical properties of pharmaceuticals are easily modified under high pressure (HP), accompanied by crystal structural changes.

Ionic liquids (ILs) are simple molecular systems that consist of a cation and an anion. Thus, the ILs possess phase varieties in the solid state. For the past two decades, the molecular conformations of cations and anions have been evaluated energetically to investigate the relationship between molecular conformations and crystal structures. Conformations of the representative 1-alkyl-3-methylimidazolium ([$C_n$mim]$^+$) cations were calculated [11–14], where n denotes the alkyl chain length. In [C_6mim]$^+$, several cationic conformations were optimized using density functional theory (DFT) calculations [14]. At $n \geq 2$, the [$C_n$mim]$^+$ cations become asymmetric. Additionally, the perfluorobutanesulfonate ($C_4F_9SO_3^-$, [PFBS]$^-$) anion has conformational degrees of freedom, and also its molecular structure is asymmetric. By the torsional potential calculation, the stable conformers of [PFBS]$^-$ were found to have *trans* and *gauche* conformation [15]. The torsional potential of [PFBS]$^-$ resembled that of [$C_4F_9BF_3$]$^-$ [16]. Using differential scanning calorimetry (DSC), it was found that [C_6mim][PFBS] as one of the fluorinated ionic liquids (fILs) crystallizes at low temperature (LT) [17,18]. On the DSC thermal traces, the complicated LT-crystal polymorphs were observed in the fILs. Furthermore, the crystal polymorphs and crystal structures of [$C_n$mim][PFBS] (n = 4, 6, and 8) were clarified using simultaneous X-ray diffraction and DSC measurements [15]. The crystal structures of [C_4mim][PFBS] and [C_8mim][PFBS] were characterized by large lattice constants at LT.

Crystal polymorphs of the ILs under HP have been examined using X-ray diffraction [19–25]. HP-crystal polymorphs of the ILs were entirely different from LT-crystal polymorphs. For [C_4mim][PFBS] [25], the HP-crystal polymorph was influenced by *gauche* conformers of both of cation and anion. In addition, relating to the conformational varieties, the crystal polymorphs and multiple pathways at both LT and HP were summarized in the literature [26,27].

In this study, the HP-crystal polymorphs and multiple pathways of [C_6mim][PFBS] were explained using X-ray diffraction. The complicated phase behavior of [C_6mim][PFBS] is represented via reentrant

* Corresponding author.

https://doi.org/10.1016/j.chemphys.2022.111479
Received 1 November 2021; Received in revised form 10 January 2022; Accepted 9 February 2022

layered structures, and the irreversible crystal polymorph was induced by the hybrid layered structure.

2. Materials and methods

The fIL used was [C_6mim][PFBS] (Kanto Chemical Co.). We used it as-received sample without further purification, as vacuum contamination easily occurred. The molecular conformations of $[PFBS]^-$ are depicted in Fig. 1. Cation [13,14] and anion [15] possess conformational degrees of freedom. The electrostatic potential map of [C_4mim][PFBS] was demonstrated using DFT calculations [15]. In $[PFBS]^-$, the anisotropic distribution of the electrostatic potential map was distinguished.

HP X-ray diffraction experiments were performed using a Mao-Bell type diamond anvil cell (DAC) in the BL-18C of the Photon Factory at the High Energy Accelerator Research Organization in Japan [28]. In a glove box with dry flowing nitrogen, the sample and ruby balls were loaded into the hole (0.25 mm) of the pre-indented stainless gasket with a thickness of 0.18 mm in the DAC. A microbeam with a diameter of 35 μm was obtained using double collimators. Two-dimensional (2D) diffraction patterns were obtained using an imaging plate (IP) system (BAS2500, Fuji-Film Co., Japan) [28]. Thus, IP was a digital X-ray film. The 2D data were converted into 1D intensity data to minimize the preferred orientation on the Debye rings. To remove air scattering, a vacuum chamber with polyimide (Kapton)-film windows was used (125 μm thickness) and the pressure was determined from the spectral shift of the R_1 fluorescence line of the ruby balls in the sample chamber of the DAC. The scattered angles 2θ and the incident wavelength, λ (= 0.08072 nm), were calibrated using a standard CeO_2 polycrystalline. The scattered wavevector, Q, is represented by $4\pi\sin(\theta)/\lambda$ (nm^{-1}), in which 2θ is the scattered angle. The crystal structures were analyzed by the combination of *FOX* [29] and *Conograph* [30]. *Conograph* was used to calculate the possible lattice parameters and space groups, and the space group was identified via global optimization using *FOX*.

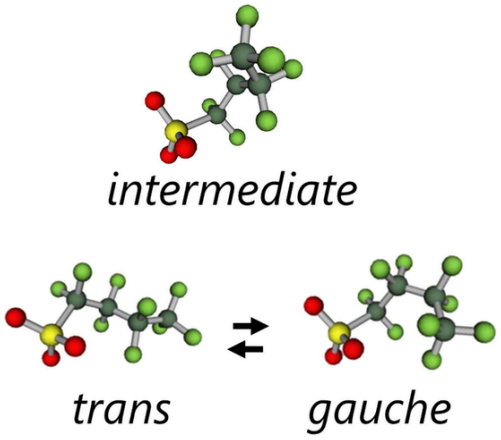

Fig. 1. Molecular structures of the $[PFBS]^-$ anion.

3. Results and discussion

Fig. 2(a) and 2(b) show the X-ray diffraction patterns of [C_6mim][PFBS] at room temperature, on compression and decompression, respectively. At ambient pressure, the prepeak in the liquid state appeared at 3.9 nm^{-1} (blue circle in Fig. 2(a) and Fig. S1(a)) [18]. The liquid density of [C_6mim][PFBS] was 1.39 (g cm^{-3}) [31]. On the other hand, the solid density of LT-crystal of [C_6mim][PFBS] was 1.481 (g cm^{-3}) [15]. On compression, crystallization occurred at 0.2 GPa with the ideal Debye ring on the IP. Bragg reflections were sharp, reflecting the high-crystallinity. Even at 0.7 GPa, diffraction pattern did not change. Here we named the HP-α phase at 0.2 and 0.7 GPa. The characteristic of HP-α phase is represented by the Bragg reflection at 3.1 nm^{-1} (one of green circles in Fig. 2(a) and Fig. S1(a)). By the structure analysis, the lowest Q peak was identified as 001 Bragg reflection. The Q po-

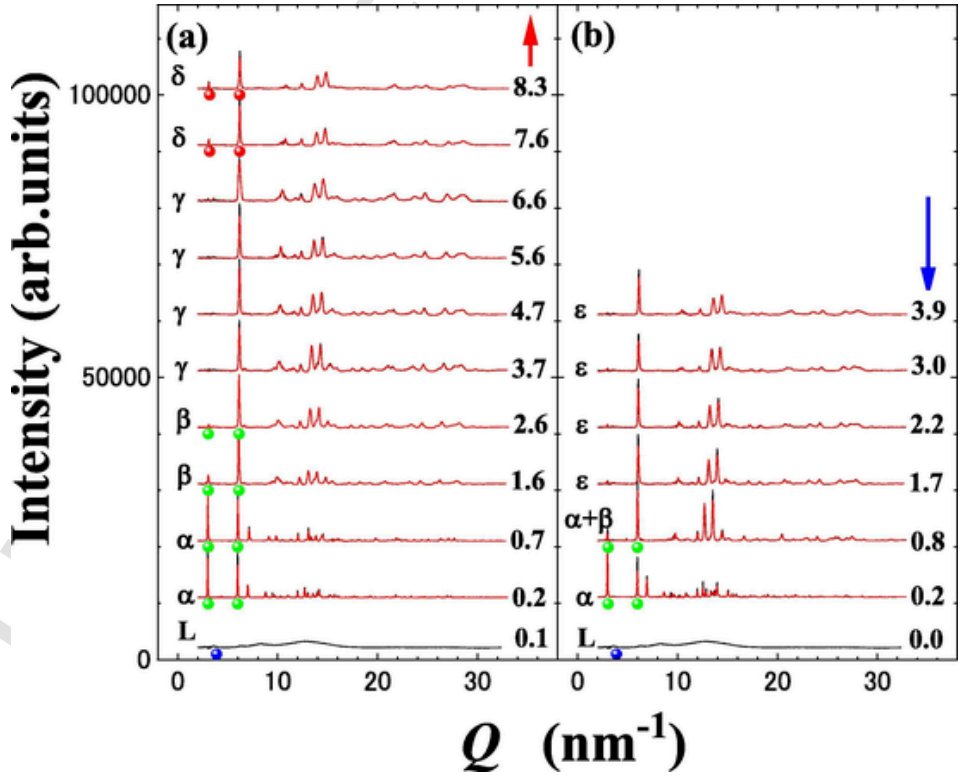

Fig. 2. X-ray diffraction patterns of [C_6mim][PFBS] upon (a) compression process and (b) decompression process. Black and red curves reveal the observed and calculated patterns, respectively. Blue circle reveals prepeak positions in the liquid state. 00ℓ Bragg reflections are expressed by red and green circles.

sition of the Bragg reflection at 3.1 nm^{-1} was different from that of pre-peak in the liquid state. Moreover, the distinct layered structure of the HP-α phase was expressed by the intense 00ℓ Bragg reflections (green circles in Fig. 2(a)). Compared with the strong 00ℓ Bragg reflections, *hk*0 Bragg reflections were weak (Fig. S2). The diffraction pattern of the HP-α phase resembles the crystal structure of 3,7,11-trimethyldodecyl tetrafluoroborate ([TMD][BF_4]), which had a liquid crystal (LC) phase at high temperature [32]. In [TMD][BF_4], sharp and strong 00ℓ Bragg reflections below 6 nm^{-1} and weak *hk*0 Bragg reflections above 6 nm^{-1} appeared. Thus, it is predicted that the HP-α phase is the LC-based layered crystal structure. X-ray structural analysis indicated that HP-α phase was triclinic ($P\bar{1}$) (Table 1). The lattice constants of HP-α phase were large despite the simple molecular system. The number of cation-anion pairs in the unit cell (*Z*) was 15. The crystal structure of HP-α phase was different from the LT-crystal structure [15]. The crystallographic feature of HP-α phase is characterized by the layered structure, stacking along the *c* direction (Fig. 3(a) and Fig. S3(a)). In the [C_6mim]$^+$ cation, many stable conformers were calculated by the DFT calculations [14]. It is quite difficult to identify the cation conformer in the unit cell, since the geometrical difference of the possible conformers is small. Thus, in this study, we focus the [PFBS]$^-$ anion, which has only two conformers. The [PFBS]$^-$ conformer ratio in the unit cell was found to be *trans*:*gauche* = 11:4. The [PFBS]$^-$ stacking layers consist both of all *trans* and mixing of *trans* and *gauche* conformers. In addition, the high-crystallinity of the HP-α phase was formed by the balance of *trans* and *gauche* of the [PFBS]$^-$ conformers. In the case of [C_4mim][PFBS], LT-crystal contained only *trans* conformer of [PFBS]$^-$ [15], although the *trans* and *gauche* conformers coexisted under HP for high molecular packing efficiency [25]. Similarly, mixing of *trans* and *gauche* conformation in [C_6mim][PFBS] was observed under HP. A long periodic lattice of the HP-α phase derived from the layering of the [PFBS]$^-$ conformer.

Table 1
Crystallographic data for [C_6mim][PFBS].

P (GPa)			spaceGroup	*a* (nm)	*b* (nm)	*c* (nm)	α(°)	β(°)	γ (°) *Z*	ρ (g/cm^3)	R_w (%)	*R* (%)
The first cycle												
0.2	α	$P\bar{1}$	1.8594	1.9872	2.1043	88.58	85.76	83.93	15	1.507	25.72	14.50
0.7	α	$P\bar{1}$	1.8567	1.9832	2.0956	88.41	85.63	83.80	15	1.519	9.42	6.49
1.6	β	$P\bar{1}$	1.3082	1.9958	2.0964	92.82	95.02	109.60	10	1.513	10.86	5.59
2.6	β	$P\bar{1}$	1.3067	1.9981	2.0982	92.78	95.12	109.65	10	1.512	10.35	5.80
2.6	γ	$P2_1$	1.0783	1.6445	1.2282	90	109.98	90	4	1.513	17.42	11.23
3.7	γ	$P2_1$	1.0751	1.6498	1.2205	90	109.96	90	4	1.522	13.62	10.35
4.7	γ	$P2_1$	1.0677	1.6500	1.2081	90	109.88	90	4	1.548	14.88	11.15
5.6	γ$P2_1$		1.0630	1.6376	1.1957	90	109.70	90	4	1.581	18.43	13.53
6.6	γ	$P2_1$	1.0730	1.6618	1.1682	90	110.43	90	4	1.587	10.17	6.89
7.6	δ	*Iba*2	0.9701	1.2166	4.0650	90	90	90	10	1.614	15.91	14.39
8.3	δ	*Iba*2	0.9710	1.2094	4.0646	90	90	90	10	1.622	14.32	10.82
3.9	ε	$P2_1$	0.8951	0.8228	2.1635	90	109.79	90	3	1.549	18.75	13.03
3.0	ε	$P2_1$	0.8950	0.8313	2.1482	90	109.43	90	3	1.541	20.07	14.60
2.2	ε	$P2_1$	0.8986	0.8348	2.1560	90	109.20	90	3	1.521	17.08	12.74
1.7	ε	$P2_1$	0.9089	0.8346	2.1583	90	109.46	90	3	1.505	19.98	16.51
0.8	β	$P\bar{1}$	1.3075	1.9957	2.0994	92.55	95.13	109.53	10	1.510	19.16	15.50
0.2	α$P\bar{1}$		1.8635	2.0072	2.1047	88.68	84.62	83.66	15	1.491	9.53	6.66
The second cycle												
0.2	α$P\bar{1}$	1.8516	1.9901	2.1106	88.77 85.85 83.69 15 1.507 23.95 18.84							
0.8	α$P\bar{1}$	1.8531	1.9939	2.1065	88.98 86.10 83.90 15 1.504 15.86 11.53							
1.2	β$P\bar{1}$	1.3086	1.9961	2.0965	92.94 94.89 109.52 10 1.511 10.46 5.32							
2.1	β$P\bar{1}$	1.3074	2.0005	2.0977	92.71 95.28 109.71 10 1.511 20.37 19.24							
2.1	γ $P2_1$	1.0535	1.6569	1.2197	90 110.19 90 4 1.550 27.35 24.06							
2.8	β$P\bar{1}$	1.3077	2.0013	2.0968	92.68 95.29 109.75 10 1.511 18.50 13.71							
2.8	γ $P2_1$	1.0515	1.6444	1.2098	90 109.67 90 4 1.572 24.51 19.33							
2.3	β$P\bar{1}$	1.3080	2.0039	2.0985	92.69 95.31 109.80 10 1.508 18.11 14.48							
2.3	γ $P2_1$	1.0522	1.6470	1.2145	90 109.82 90 4 1.564 20.80 17.02							
1.3	α$P\bar{1}$	1.8516	1.9826	2.0924	88.42 85.67 83.74 15 1.526 23.49 21.01							
1.3	β$P\bar{1}$	1.3111 2.0123 2.0932 92.57 95.41 109.85 10 1.502 24.01 22.98										
0.5	α$P\bar{1}$	1.8534	1.9987	2.1068	88.96 86.10 83.87 15 1.500 20.80 17.40							
0.5	β$P\bar{1}$	1.3112	2.0155	2.0923	92.86 95.27 110.03 10 1.503 23.34 19.97							
0.2	α$P\bar{1}$	1.8591	1.9892	2.1072	88.80 85.88 83.65 15 1.504 17.97 16.19							

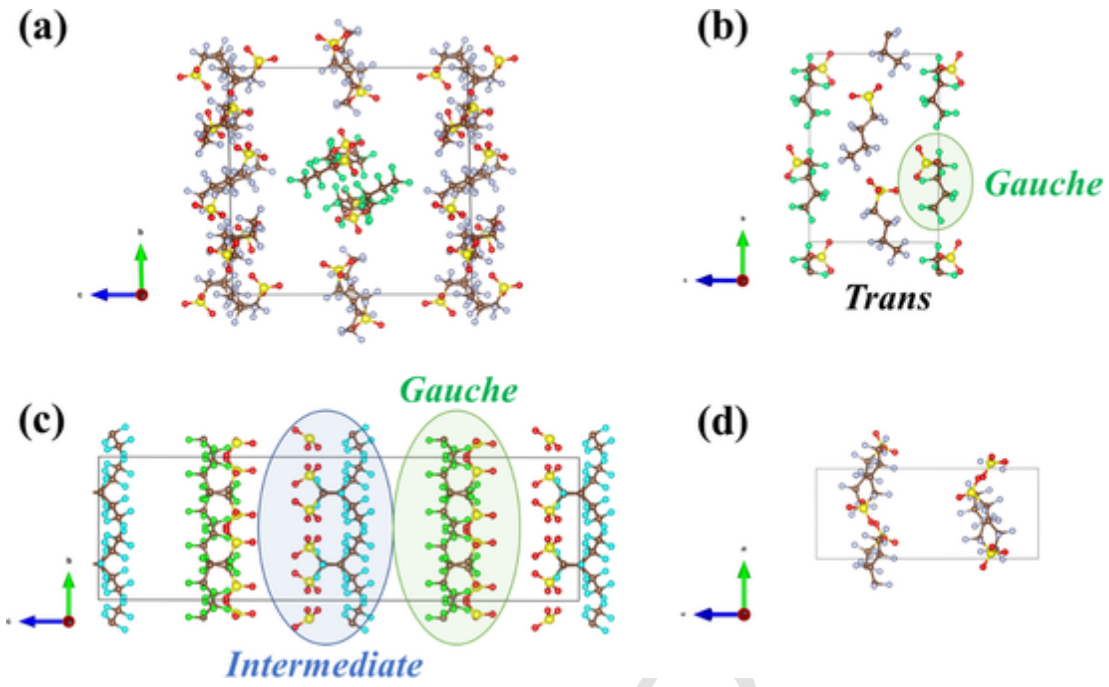

Fig. 3. Unit cell of (a) HP-α phase (0.7 GPa), (b) HP-γ phase (3.7 GPa), (c) HP-δphase (8.3 GPa) upon compression, and (d) HP-ε phase (3.9 GPa) upon decompression. $[C_6mim]^+$ was omitted to enhance the conformers of $[PFBS]^-$. To distinguish the *gauche* and *intermediate* conformers of $[PFBS]^-$ from *trans* one, green colored F (*gauche*) and light blue colored F (*intermediate*) are used.

Upon further compression, the subsequent phase transition was observed at 1.6 GPa. HP-β phase appeared with decreased peak intensity (3.1 nm^{-1}) and disappearing Bragg reflections (Fig. 2(a)). Large lattice constants of HP-β phase were obtained by the structure analysis (Table 1). Here, we noticed that HP-α and HP-β phases are described by 00ℓ Bragg reflections, representing the layered structures. The space group of HP-β phase was also triclinic ($P\bar{1}$), although the lattice constants of HP-β phase were different from those of HP-α phase. Large unit cells of HP-α and HP-β phases having the 3.1 nm^{-1} peak are classified as *layering* I state, which is characterized by the layered structure resembling the LC structure. At 2.6 GPa, 001 Bragg reflection at 3.1 nm^{-1} decreased remarkably, but still existed (Fig. 2(a) and Fig. S1(a)). In spite of the weak peak intensity of the 001 Bragg reflection, HP-β phase was identified at 2.6 GPa (Table 1). For a comparison, the X-ray diffraction pattern at 2.6 GPa was calculated using higher-pressure phase (HP-γ phase) as listed in Table 1. The worse reliability factors (R_w and R) using the HP-γ phase implies that, at 2.6 GPa, HP-β phase existed.

Drastic phase transition was observed on the IP at 3.7 GPa ($=P_1$). As shown in Fig. 2(a) and Fig. S1(a), the 3.1 nm^{-1} peak completely disappeared at P_1. This means that the long periodic layered structure vanished. Additionally, peak broadening of Bragg reflections became dominant. Thus, the lattice distortion was induced under HP. The discrete phase transition is explained by the small unit cell and monoclinic ($P2_1$) as HP-γ phase (Table 1). Therefore, P_1 is characterized by the phase transition from triclinic to monoclinic with losing the long periodicity. Moreover, in the unit cell, the $[PFBS]^-$ conformer ratio became *trans*:*gauche* = 1:1 with losing layering (Fig. 3(b) and Fig. S3(b)). Obviously, *gauche* conformer of $[PFBS]^-$ increased in the unit cell. In general, in a flexible molecular system, a non-global minimum conformer was formed in a crystal with high strain energy [33]. Here, we assume that the *gauche* conformer of $[PFBS]^-$ contributes to efficient molecular packing, but the folding *gauche* causes the orientational disorder. The assumption can explain the experimental results at P_1. By a competition between lattice energy and strain, the small unit cell of the HP-γ phase could be preferred with permitting the lattice distortion. By increasing pressure up to 6.6 GPa, HP-γ phase did not transform to the other phase.

At 7.6 GPa ($=P_2$), reentrant behavior of phase transition was observed distinctly. This is because the low-*Q* peak marked by the red circle (Fig. 2(a) and Fig. S1(a)) appeared again at P_2. Although the 00ℓ Bragg reflections indicated the long periodic layered structure, the space group of the new phase was orthorhombic (Table 1). Thus, we call this the HP-δ phase above P_2. Thus, P_2 is represented by the monoclinic-orthorhombic phase transition. Hence, in the ILs, first, we observed the reentrant phase behavior: HP-α and HP-β below P_1 (*layering* I) and HP-δ above P_2 (*layering* II). In the unit cell of the HP-δ phase, the layers of $[PFBS]^-$ are stacking along the *c*-direction (Fig. 3(c) and Fig. S3(c)), suggesting drastic molecular rearrangement of cation and anion at P_2. However, the hybrid layered structure consisted of two layers: one is occupied only by the *intermediate* conformer of $[PFBS]^-$, and the other is the *gauche* conformers of $[PFBS]^-$. The torsion angle of the *intermediate* conformer is 100° (Fig. 1) and those of *trans* and *gauche* are 150° and 60°, respectively [15]. It should be noticed that the barrier between *trans* and *gauche* was estimated to be 1.4 kcal/mol. Although the torsional potential of the *intermediated* conformer of $[PFBS]^-$ is relatively high, distorted molecular geometries are selected in a close-packed environment against the non-global minimum lattice energy [33]. In addition, we emphasized that the *intermediated* conformer of $[PFBS]^-$ is regarded as an HP-inherent conformer. In a previous study [22], an energetically unstable planar' (*P*') conformer of $[C_2mim]^+$ appeared only under HP. Further, HP-driven *P*' conformer caused the large unit cell with the low-*Q* peak. In the unit cell of the HP-δ phase, the $[PFBS]^-$ conformer ratio was *intermediate*:*gauche* = 1:1, and the *intermediated* conformer layer and the *gauche* conformer layer are stacking alternately (Fig. 3(c) and Fig. S3(c)). Thus, the HP-δ phase described by the hybrid layers is identified as the *layering* II state. HP-hybrid layered structure was observed in $[C_{10}mim][Cl]$ [21]. In the case of $[C_{10}mim][Cl]$, there are no anionic conformation degrees of freedom. Therefore, the HP-hybrid layered structure was derived from the $[C_{10}mim]^+$ conformers. The maximum pressure (P_{max}) was 8.3 GPa in the first pressure cycle. Upon compression, the HP-phase behavior of $[C_6mim][PFBS]$ was characterized as the reentrant phase transition (*layering* I and *layering* II) in addition to the HP-crystal polymorph. The reentrant behavior is expressed by 00ℓ Bragg reflections and the hybrid layers of $[PFBS]^-$.

Phase changes upon decompression were examined to clarify whether crystal polymorph is reversible or irreversible. The decompression-induced phase transition was detected at 3.9 GPa (Fig. 2(b) and Fig. S1(b)). The low-Q peak of the Bragg reflection vanished and new peaks appeared. The new crystal phase did not coincide with the crystal phases upon compression. Thus, this new phase, HP-ε phase, was an irreversible phase transition. The space group of HP-ε phase was monoclinic ($P2_1$) (Table 1). The unit cell of HP-ε phase is shown in Fig. 3(d) and Fig. S3(d). In contrast to the other phases, no *gauche* conformer of $[PFBS]^-$ was found in the unit cell of the HP-ε phase. The spatially packed $[PFBS]^-$ *gauche* returned to the *trans* conformer because of the lattice relaxation upon decompression. The irreversible phase transition could be derived from the *layering* II state above P_2. The HP-ε phase without the $[PFBS]^-$ *gauche* conformer existed with decreasing pressure down to 1.7 GPa. At 0.8 GPa, a weak but sharp Bragg reflection appeared again at the low-Q position. As shown in Table 1, the new phase is equivalent to HP-β phase upon compression. Compared with diffraction pattern of the HP-β phase upon compression, Bragg intensities and peak widths were different at 0.8 GPa upon decompression. Peak broadening and a slightly different diffraction pattern at high Q region could be caused by the phase coexistence (α and β phases). While, the different Bragg intensity ratios were derived from partial preferred orientation of the Debye rings upon compression and ideal Debye rings upon decompression on the IP (Figs. S4(a) and S4(b)). Reversely appeared HP-β phase (*layering* I) suggests that reentrant phase transition also occurred upon decompression. Finally, at 0.2 GPa, quite sharp Bragg reflections were observed with increasing low-Q peak intensity. The crystal was found to be the HP-α phase but not the HP-β phase. Intensity ratios of the HP-α phase upon decompression did not coincide with those upon compression. As mentioned earlier, the discrepancy upon compression and decompression was originated from the preferred orientation of the Debye rings (Figs. S5(a) and 5(b)). At ambient pressure, the sample of $[C_6mim][PFBS]$ easily melted.

HP-multiple pathways occurred accompanying with HP-crystal polymorph. For instance, multiple pathways of $[C_2mim][NO_3]$ were due to the presence/absence of the HP-inherent conformer (P') of $[C_2mim]^+$ [22]. Thus, we performed the second pressure cycle, where the P_{max} was 2.8 GPa below P_1. Fig. 4(a) and 4(b) indicate X-ray diffraction patterns in the second cycle upon compression and decompression, respectively. Similar to the first pressure cycle, the subsequent phase changes (α-β phases) upon compression were observed even in the second cycle (Fig. 4(a)). Owing to the preferred orientation of the Debye rings (Fig. S6(b)), the detailed intensity ratios in the second pressure cycle were different from those in the first pressure cycle. Both at 2.1 GPa and 2.8 GPa upon compression, the weak 001 Bragg reflection was detected even in the second cycle (Fig. 4(a)). The smaller R_w and R values in Table 1 also support the HP-β phase in the second cycle. By preventing the β-γ phase transition at P_1, we reduced pressure not to exceed P_1. Upon decompression, the HP-β phase existed down to 2.3 GPa. At 1.3 GPa, X-ray diffraction pattern was fitted even using the lattice parameters of the HP-α phase (Table 1). Below 1 GPa, it was found by an optical microscope that crystal domains changed drastically. It was evident from the diffraction pattern (Fig. 4(b)) that the HP-β and HP-α phases coexist at 0.5 GPa considering the comparable reliability factors (Table 1). Due to the difficulty in pressure manipulation upon decompression, we could not obtain a single phase at a low-pressure region. However, by careful pressure treatment, we probe a single phase of HP-α phase at 0.2 GPa. Simultaneously, the morphology of the crystal domains was modified by the appearance of HP-α phase. Without the phase transition from triclinic to monoclinic at P_1 upon compression, reversible HP-phase transition of $[C_6mim][PFBS]$ was realized by removing the influence of HP-γ phase with losing the layered structure.

The complicated HP-phase behaviors of $[C_6mim][PFBS]$ are illustrated in Fig. 5. The HP-phase diversity of $[C_6mim][PFBS]$ is originated from the following phenomena; (i) reversible/irreversible crystal polymorph, (ii) reentrant phase behavior with layered structures, (iii) the HP-inherent $[PFBS]^-$ *intermediate* conformer, and (iv) multiple pathways of phase transition. Focusing on (i), the HP-crystal polymorph of $[C_6mim][PFBS]$ is different from the LT-one [15]. The $[PFBS]^-$ *gauche* conformer promotes the molecular packing efficiency under HP. Above

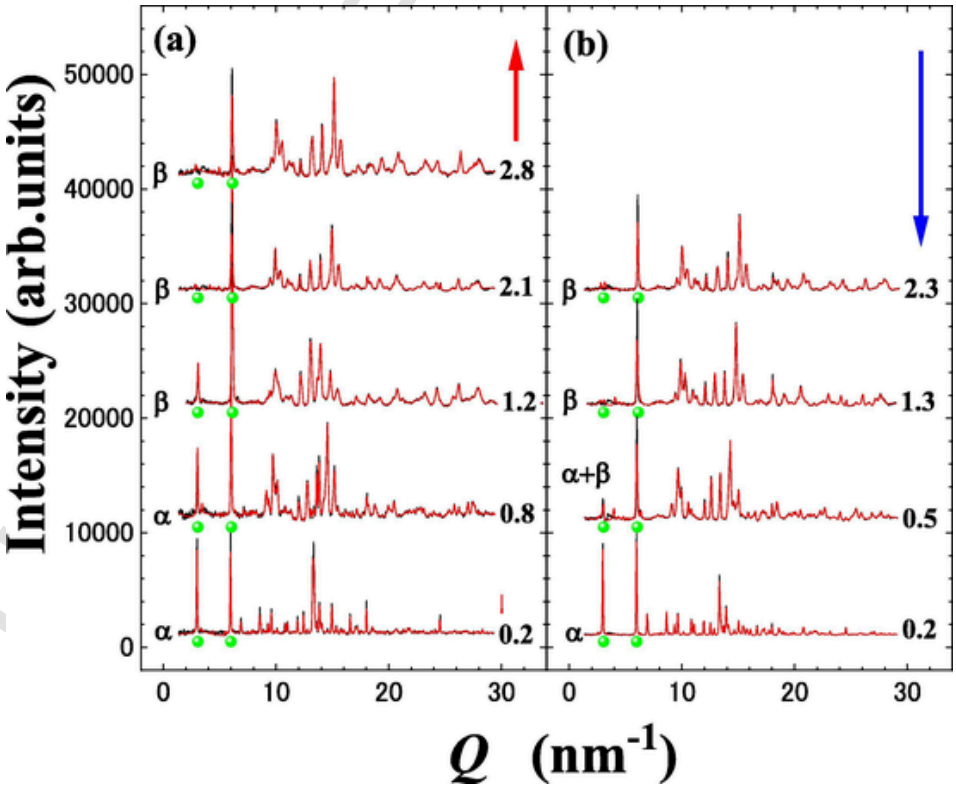

Fig. 4. X-ray diffraction patterns below 3.0 GPa. 00ℓ Bragg reflections are expressed by red and green circles.

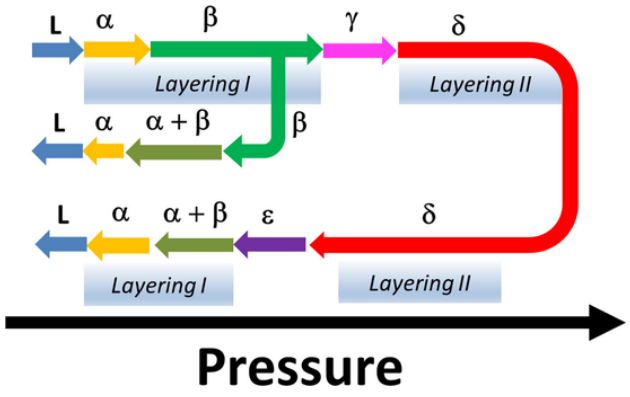

Fig. 5. Schematic crystal polymorph and multiple pathways of [C_6mim][PFBS] under HP.

P_2, unstable [PFBS]$^-$ *intermediate* conformer exists, and contributes to the hybrid layered structure. Thus, in the case of (ii), HP-reentrant phase behavior was first observed in [C_6mim][PFBS]. In general, the reentrant phase transition is seen in a frustrated spin system [34]. Also, in LC as a molecular system, multiple reentrant phase behaviors of nematic and smectic phases occurred, and its complexity was influenced extensively by the molecular tail length [35]. Frustration is caused by competition between ferro- and antiferro-like interactions. More interestingly, nanoconfined ILs exhibited the reentrant phase behaviors [36]. By breaking the Coulombic ordering, symmetry changes were demonstrated. In this study, *layering* II of [C_6mim][PFBS] is regarded as a frustrating system. The frustration is represented by a hybrid layered structure of the competing [PFBS]$^-$ *intermediate* and *gauche* conformers. In addition, we insist that molecular flexibility and conformational degrees of freedom of [PFBS]$^-$ provide an intrinsic property of the reentrant phase behavior. In (iii) and (iv), the [PFBS]$^-$ *intermediate* conformer triggers the HP-ε phase upon decompression without the [PFBS]$^-$ *gauche* conformer. The *intermediate* conformer as a non-global minimum is connected with the irreversible crystal polymorph. Alternatively, reversible crystal polymorph was realized below P_1.

4. Summary

Reentrant phase transition of [C_6mim][PFBS] under HP was observed via X-ray diffraction. The reentrant behavior is described by the simple layering of [PFBS]$^-$ (*trans* and *gauche*) and hybrid layered structure (*intermediate* and *gauche*). The presence/absence of HP-inherent [PFBS]$^-$ *intermediate* conformer caused HP-ε phase upon decompression, which shows an irreversible phase transition. The HP-crystal polymorph accompanied by changing the *gauche* conformer ratio was different from the LT-crystal polymorph without the *gauche* ones. The complicated HP-phase transitions, such as the reentrant layering, crystal polymorphs, and multiple pathways, indicate that conformational degrees of freedom of [PFBS]$^-$ cause frustration in the well-packed crystal lattice. Under HP, the distorted molecular geometry is preferred without energy cost on the conformational energy landscape.

Uncited references

[11,12],.

CRediT authorship contribution statement

Hiroshi Abe: Conceptualization, Writing – original draft, Writing – review & editing. **Yoshihiro Koyama:** Data curation. **Seiya Shimono:** Data curation. **Hiroaki Kishimura:** Data curation. **Kiyoto Matsuishi:** Data curation.

Declaration of Competing Interest

The authors declare that they have no known competing financial interests or personal relationships that could have appeared to influence the work reported in this paper.

Acknowledgments

We appreciate Dr. T. Takekiyo, Prof. Y. Yoshimura of National Defense Academy, and Prof. N. Hamaya of Ochanomizu University for helpful discussions. We acknowledge the support of Photon Factory (Proposal Nos. 2017G021 and 2019G006). *VESTA* 3 was used for displaying crystal structures [37].

References

[1] A.J. Cruz-Cabeza, J. Bernstein, Conformational polymorphism, Chem. Rev. 114 (4) (2014) 2170–2191.
[2] H. Bergeron, D. Lebedev, M.C. Hersam, Polymorphism in post-dichalcogenide two-dimensional materials, Chem. Rev. 121 (2021) 2713–2775.
[3] A.J. Cruz-Cabeza, N. Feeder, R.J. Davey, Open questions in organic crystal polymorphism, Commun. Chem. 3 (2020) 142–144.
[4] K.M. Steed, J.W. Steed, Packing problems: high Z′ crystal structures and their relationship to cocrystals, inclusion compounds, and polymorphism, Chem. Rev. 115 (2015) 2895–2933.
[5] S.L. Price, Why don't we find more polymorphs? Acta Cryst. B 69 (4) (2013) 313–328.
[6] G.J.O. Beran, Modeling polymorphic molecular crystals with electronic structure theory, Chem. Rev. 116 (2016) 5567–5613.
[7] S.L. Price, From crystal structure prediction to polymorph prediction: interpreting the crystal energy landscape, Phys. Chem. Chem. Phys. 10 (15) (2008) 1996, https://doi.org/10.1039/b719351c.
[8] S.L. Price, D.E. Braun, S.M. Reutzel-Edens, Can computed crystal energy landscapes help understand pharmaceutical solids? Chem. Commun. 52 (44) (2016) 7065–7077.
[9] M.A. Neumann, J. van de Streek, F.P.A. Fabbiani, P. Hidber, O. Grassmann, Combined crystal structure prediction and high-pressure crystallization in rational pharmaceutical polymorph screening, Nat. Commun. 6 (2015) 7793–7797.
[10] J. Hoja, H.-Y. Ko, M.A. Neumann, R. Car, R.A. DiStasio Jr., A. Tkatchenko, Reliable and practical computational description of molecular crystal polymorphs, Sci. Adv. 5 (2019) 3338–3339.
[11] J.N. Canongia Lopes, J. Deschamps, A.A.H. Pádua, Modeling ionic liquids using a systematic all-atom force field, J. Phys. Chem. B 108 (6) (2004) 2038–2047.
[12] S. Tsuzuki, A.A. Arai, K. Nishikawa, Conformational analysis of 1-butyl-3-methylimidazolium by CCSD(T) level ab initio calculations: effects of neighboring anions, J. Phys. Chem. B 112 (26) (2008) 7739–7747.
[13] J. Kiefer, C.C. Pye, Structure of the room-temperature ionic liquid 1-hexyl-3-methylimidazolium hydrogen sulfate: conformational isomerism, J. Phys. Chem. A 114 (24) (2010) 6713–6720.
[14] T. Endo, T. Higuchi, Y. Kimura, DFT study on conformation of 1-alkyl-3-methylimidazolium with ethyl, propyl, butyl, pentyl, and hexyl group, Bull. Chem. Soc. Jpn. 93 (6) (2020) 720–729.
[15] Y. Koyama, S. Shimono, H. Abe, K. Matsuishi, Crystal polymorphs in 1-alkyl-3-methylimidazolium perfluorobutanesulfonate ionic liquids, J. Mol. Liq. 317 (2020) 113908–113917.
[16] S. Tsuzuki, T. Umecky, H. Matsumoto, W. Shinoda, M. Mikami, Interactions of perfluoroalkyltrifluoroborate anions with Li ion and imidazolium cation: effects of perfluoroalkyl chain on motion of ions in ionic liquids, J. Phys. Chem. B 114 (2010) 11390–11396.
[17] A.B. Pereiro, M.J. Pastoriza-Gallego, K. Shimizu, I.M. Marrucho, J.N. Canongia Lopes, M.M. Piñeiro, L.P.N. Rebelo, On the formation of a third, nanostructured domain in ionic liquids, J. Phys. Chem. B 117 (2013) 10826–10833.
[18] M.L. Ferreira, M.J. Pastoriza-Gallego, J.M.M. Araújo, J.N. Canongia Lopes, L.P.N. Rebelo, M.M. Piñeiro, K. Shimizu, A.B. Pereiro, Influence of nanosegregation on the phase behavior of fluorinated ionic liquids, J. Phys. Chem. C 121 (2017) 5415–5427.
[19] H. Abe, T. Takekiyo, N. Hatano, M. Shigemi, N. Hamaya, Y. Yoshimura, Pressure-induced frustration–frustration process in 1-butyl-3-methylimidazolium hexafluorophosphate, a room-temperature ionic liquid, J. Phys. Chem. B 118 (2014) 1138–1145.
[20] H. Abe, Y. Imai, T. Takekiyo, Y. Yoshimura, N. Hamaya, Low temperature and high pressure crystals of room temperature ionic liquid: *N*, *N*-diethyl-*N*-methyl-*N*-(2-methoxyethyl) ammonium tetrafluoroborate, IOP Conf. Ser.: Mater. Sci. Eng. 54 (2014) 012003–012007.
[21] H. Abe, N. Hamaya, Y. Koyama, H. Kishimura, T. Takekiyo, Y. Yoshimura, D. Wakabayashi, N. Funamori, K. Matsuishi, Long periodic structure of a room-temperature ionic liquid by high-pressure small-angle X-ray scattering and wide-angle X-ray scattering: 1-decyl-3-methylimidazolium chloride, ChemPhysChem 19 (2018) 1441–1447.
[22] H. Abe, T. Takekiyo, Y. Yoshimura, N. Hamaya, S. Ozawa, Crystal polymorphs and multiple crystallization pathways of highly pressurized 1-ethyl-3-

methylimidazolium nitrate, Aust. J. Chem. 72 (2) (2019) 87, https://doi.org/10.1071/CH18368.
[23] H. Abe, H. Kishimura, T. Takekiyo, T. Hanasaki, Y. Yoshimura, N. Hamaya, Low-temperature and high-pressure phase changes of room temperature ionic liquids, J. Mol. Liq. 300 (2020) 112340–112349.
[24] H. Abe, Y. Koyama, H. Kishimura, K. Matsuishi, High-pressure crystal polymorph of the protic ionic liquid: ethylammonium nitrate, J. Mol. Liq. 318 (2020) 113959–113966.
[25] Y. Koyama, S. Shimono, H. Kishimura, T. Takekiyo, Y. Yoshimura, H. Abe, K. Matsuishi, High-pressure crystal polymorphs in 1-butyl-3-methylimidazolium perfluorobutanesulfonate, J. Mol. Liq. 335 (2021) 116415–116417.
[26] H. Abe, H. Kishimura, T. Takekiyo, Y. Yoshimura, N. Hamaya, Non-equilibriumprotic and aprotic ionic liquids: measuring the distance from the equilibrium state, J. Mol. Liq. 283 (2019) 196–207.
[27] H. Abe, Phase variety in ionic liquids: Hydrogen bonding and molecular conformations, J. Mol. Liq. 332 (2021) 115189–115227.
[28] O. Shimomura, K. Takemura, H. Fujihisa, Y. Fujii, Y. Ohishi, T. Kikegawa, Y. Amemiya, T. Matsushita, Application of an imaging plate to high-pressure x-ray study with a diamond anvil cell, Rev. Sci. Instrum. 63 (1992) 967–973.
[29] V. Favre-Nicolin, R. Cerny, FOX, 'free objects for crystallography': a modular approach to ab initio structure determination from powder diffraction, J. Appl. Cryst. 35 (2002) 734–743.
[30] R. Oishi-Tomiyasu, Robust powder auto-indexing using many peaks, J. Appl. Cryst. 47 (2) (2014) 593–598.
[31] N.S.M. Vieira, P.M. Reis, K. Shimizu, O.A. Cortes, I.M. Marrucho, J.M.M. Araújo, J.M.S.S. Esperança, J.N.C. Lopes, A.B. Pereiro, L.P.N. Rebelo, A thermophysical and structural characterization of ionic liquids with alkyl and perfluoroalkyl side chains, RSC Adv. 5 (80) (2015) 65337–65350.
[32] P.H.J. Kouwer, T.M. Swager, Synthesis and mesomorphic properties of rigid-core ionic liquid crystals, J. Am. Chem. Soc. 129 (45) (2007) 14042–14052.
[33] H.P.G. Thompson, G.M. Day, Which conformations make stable crystal structures? Mapping crystalline molecular geometries to the conformational energy landscape, Chem. Sci. 5 (8) (2014) 3173–3182.
[34] M. Li, I. Rousochatzakis, N.B. Perkins, Reentrant incommensurate order and anomalous magnetic torque in the Kitaev magnet β-Li_2IrO_3, Phys. Rev. Res. 2 (2020) 033328–033329.
[35] J.O. Indekeu, A. Nihat Berker, Molecular structure and reentrant phases in polar liquid crystals, J. Phys. France 49 (2) (1988) 353–362.
[36] S. Mossa, Re-entrant phase transitions and dynamics of a nanoconfined ionic liquid, Phys. Rev. X 8 (2018) 031062–031115.
[37] K. Momma, F. Izumi, *VESTA* 3 for three-dimensional visualization of crystal, volumetric and morphology data, J. Appl. Cryst. 44 (2011) 1272–1276.